Earth, Moon, and Planets (2006) 99:131–146
DOI 10.1007/s11038-006-9120-8

Experimental Study of Geoneutrinos with KamLAND

SANSHIRO ENOMOTO
Research Center for Neutrino Science, Tohoku University, Aramaki Aoba, Aobaku, Miyagi, Sendai, 980-8578, Japan
(E-mail: sanshiro@awa.tohoku.ac.jp)

(Received 10 June 2006; Accepted 22 August 2006)

Abstract. The Kamioka liquid scintillator antineutrino detector (KamLAND), which consists of 1000 tones of ultra-pure liquid scintillator surrounded by 1879 photo-multiplier tubes (PMT), is the first detector sensitive enough to detect geoneutrinos. Earth models suggest that KamLAND observes geoneutrinos at a rate of 30 events/10^{32}-protons/year from the ^{238}U decay chain, and 8 events/10^{32}-protons/year from the ^{232}Th decay chain. With 7.09×10^{31} proton-years of detector exposure and detection efficiency of 0.687 ± 0.007, the 'rate-only' analysis gives 25^{+19}_{-18} geoneutrino candidates. Assuming a Th/U mass concentration ratio of 3.9, the 'rate + shape' analysis gives the 90% confidence interval for the total number of geoneutrinos detected to be from 4.5 to 54.2. This result is consistent with predictions from the Earth models. The 99% C.L. upper limit is set at 1.45×10^{-31} events per target proton per year, which is 3.8 times higher than the central value of the model prediction that gives 16 TW of radiogenic heat production from ^{238}U and ^{232}Th. Although the present data have limited statistical power, they provide by direct means an upper limit for the Earth's radiogenic heat of U and Th.

Keywords: Geoneutrino, KamLAND, earth energetics, bulk silicate earth

1. Neutrino Geophysics with KamLAND

It is widely accepted that radiogenic heat contributes a large part to the Earth's heat budget. Due to direct relation between the number of radioactive decays in the Earth and the neutrino flux from the decays, neutrinos are expected to provide fruitful information on Earth's energetics. Using neutrinos to study processes inside the Earth was first suggested by Eder (1966) and Marx (1969) in 1960's, and has been reviewed a number of times (Avilez et al., 1981; Krauss et al., 1984; Kobayashi and Fukao, 1991; Raghavan et al., 1998; Rothschild et al., 1998; Mantovani et al., 2004). The Kamioka liquid scintillator antineutrino detector (KamLAND), which detects few MeV of electron antineutrinos with 1000 tones of ultra-pure liquid scintillator, is the first detector sensitive enough to measure geologically produced antineutrinos (geoneutrinos).

^{238}U, ^{235}U and ^{232}Th generate radiogenic heat via a series of alpha and beta decays. ^{40}K generates radiogenic heat via either beta decay or electron

capture with branching ratios of 0.893 and 0.107, respectively. In addition to a daughter nucleus, each beta decay produces an electron and an antineutrino. Electron capture produces a neutrino and a daughter nucleus. These decays can be summarized by

$$\begin{aligned}
^{238}\mathrm{U} &\rightarrow {}^{206}\mathrm{Pb} + 8\,{}^{4}\mathrm{He} + 6\mathrm{e}^{-} + 6\bar{\nu}_{\mathrm{e}} + 51.7\mathrm{MeV}, \quad \tau_{1/2} = 4.468 \times 10^{9}\ \mathrm{yr} \\
^{235}\mathrm{U} &\rightarrow {}^{207}\mathrm{Pb} + 7\,{}^{4}\mathrm{He} + 4\mathrm{e}^{-} + 4\bar{\nu}_{\mathrm{e}} + 46.0\ \mathrm{MeV}\ , \quad \tau_{1/2} = 7.038 \times 10^{8}\ \mathrm{yr} \\
^{232}\mathrm{Th} &\rightarrow {}^{208}\mathrm{Pb} + 6\,{}^{4}\mathrm{He} + 4\mathrm{e}^{-} + 4\bar{\nu}_{\mathrm{e}} + 42.7\ \mathrm{MeV}\ , \quad \tau_{1/2} = 1.405 \times 10^{10}\ \mathrm{yr} \\
^{40}\mathrm{K} &\rightarrow {}^{40}\mathrm{Ca} + \mathrm{e}^{-} + \bar{\nu}_{\mathrm{e}} + 1.31\ \mathrm{MeV}\ (89.3\%), \quad \tau_{1/2} = 1.277 \times 10^{9}\ \mathrm{yr} \\
^{40}\mathrm{K} + \mathrm{e}^{-} &\rightarrow {}^{40}\mathrm{Ar} + \nu_{\mathrm{e}} + 1.51\ \mathrm{MeV}\ (10.7\%)
\end{aligned} \tag{1}$$

Antineutrino luminosity $L_{\bar{\nu}}$ (number of antineutrino emissions per unit time) and heat generation H of ^{238}U, ^{235}U, ^{232}Th and ^{40}K can be directly calculated from their mass M by

$$\begin{aligned}
^{238}\mathrm{U} &: L_{\bar{\nu}}[1/\mathrm{sec}] = 7.46 \times 10^{7} \cdot M[\mathrm{kg}] = 7.84 \times 10^{11} \cdot H[\mathrm{W}] \\
^{235}\mathrm{U} &: L_{\bar{\nu}}[1/\mathrm{sec}] = 3.20 \times 10^{8} \cdot M[\mathrm{kg}] = 5.67 \times 10^{11} \cdot H[\mathrm{W}] \\
^{232}\mathrm{Th} &: L_{\bar{\nu}}[1/\mathrm{sec}] = 1.62 \times 10^{7} \cdot M[\mathrm{kg}] = 6.18 \times 10^{11} \cdot H[\mathrm{W}] \\
^{40}\mathrm{K} &: L_{\bar{\nu}}[1/\mathrm{sec}] = 2.31 \times 10^{8} \cdot M[\mathrm{kg}] = 8.18 \times 10^{12} \cdot H[\mathrm{W}]
\end{aligned} \tag{2}$$

where the neutrino kinetic energy is subtracted from H, since almost all this energy escapes the Earth. In order to calculate the energies taken by neutrinos on beta decays, the allowed beta transition formula with the Fermi correction is used except for ^{40}K and ^{210}Bi in the ^{238}U series; the 3rd unique forbidden transition formula is used for ^{40}K, and the spectrum tabulated in (Aleksankin, 1989) is used for ^{210}Bi. The isotope decay data used in this calculation is taken from (Firestone and Shirley, 1996). Based on chondritic abundances and cosmochemical consideration of the volatility of elements, the current model of the bulk silicate Earth (BSE) (McDonough and Sun, 1995) gives heat generation of 8 TW by ^{238}U and ^{235}U, 8 TW by ^{232}Th, and 3 TW by ^{40}K, resulting in total of 20 TW for the radiogenic heat generated in the Earth's interior. Table I summarizes the neutrino luminosity, heat generation of these elements, among with total mass in the Earth given by the BSE model. Figure 1 shows the calculated antineutrino spectra from these elements. There are even more radioactive elements in the Earth, as also listed in Table I, making negligible contribution to the total radiogenic heat production.

The neutrino flux at a position $\vec{r}$ for each isotope can be calculated from the isotope distribution (isotope mass per unit rock mass) $a(\vec{r})$ by integrating the contribution over the entire Earth,

TABLE I

Radiogenic heat and geoneutrino luminosity. ^{238}U, ^{235}U and ^{232}Th represent the whole decay chains, ^{40}K to ^{187}Re are beta-decaying or electron-capture (EC) isotopes, ^{123}Te is EC only, and ^{152}Gd to ^{186}Os are alpha-decaying isotopes. $M_{\mathrm{Earth}} = 5.97 \times 10^{24}$ kg, $M_{\mathrm{BSE}} = 4.05 \times 10^{24}$ kg, and $M_{\mathrm{Core}} = 1.93 \times 10^{24}$ kg is used

Isotope	Isotope abundance (%)	H/M_{Isotope} (μW/kg)	$L_{\bar{\nu}}/M_{\mathrm{Isotope}} \times 10^7$ (1 s^{-1} kg^{-1})	BSE (Core) Model prediction		
				a_{element} (ppm)	Total H (TW)	Total $L_{\bar{\nu}} \times 10^{24}$ (1 s^{-1})
^{238}U	99.28	95.2	7.46	0.02	7.7	6.0
^{232}Th	100	26.3	1.62	0.08	8.5	5.2
^{235}U	0.72	564	3.20	0.02	0.33	0.19
^{40}K	0.0117	28.2	2.31	240	3.2	2.6
^{176}Lu	2.59	2.5×10^{-1}	2.0×10^{-1}	0.068	1.8×10^{-3}	1.4×10^{-2}
^{115}In	95.7	6.4×10^{-6}	2.6×10^{-5}	0.01	2.5×10^{-7}	1.0×10^{-5}
^{113}Cd	12.22	1.8×10^{-7}	1.3×10^{-6}	0.04 (0.15)	3.6×10^{-9} (6.5×10^{-9})	2.5×10^{-7}(4.5×10^{-7})
^{87}Rb	27.835	4.2×10^{-2}	3.2×10^{-1}	0.60	2.8×10^{-2}	2.2
^{138}La	0.0902	1.8×10^{-1}	3.1×10^{-2}	0.65	4.3×10^{-4}	7.4×10^{-4}
^{187}Re	62.6	1.3×10^{-4}	1.6×10^{-1}	0.0003 (0.23)	1.0×10^{-7}(3.6×10^{-5})	1.2×10^{-3} (4.5×10^{-1})
^{123}Te	0.908	0	0	0.012 (0.85)	0 (0)	0 (0)
^{152}Gd	0.20	2.8×10^{-4}	0	0.54	1.2×10^{-6}	0
^{148}Sm	11.3	4.1×10^{-6}	0	0.41	7.6×10^{-7}	0
^{144}Nd	23.8	1.2×10^{-5}	0	1.25	1.5×10^{-5}	0
^{147}Sm	15.0	3.1×10^{-1}	0	0.41	7.8×10^{-2}	0
^{174}Hf	0.162	1.5×10^{-5}	0	0.28	2.8×10^{-8}	0
^{190}Pt	0.01	5.6×10^{-2}	0	0.007 (5.7)	1.6×10^{-7} (6.1×10^{-5})	0 (0)
^{186}Os	1.58	1.6×10^{-5}	0	0.003 (2.8)	3.1×10^{-9} (1.4×10^{-6})	0 (0)

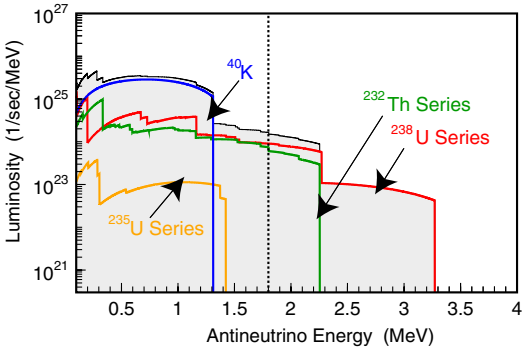

Figure 1. Geoneutrino Spectrum. KamLAND can only detect geoneutrinos with energies greater than 1.8 MeV (right of the vertical dotted line); hence it is insensitive to ^{235}U and ^{40}K geoneutrinos.

$$\frac{\mathrm{d}\Phi(E_\nu,\vec{r})}{\mathrm{d}E_\nu} = A\frac{\mathrm{d}n(E_\nu)}{\mathrm{d}E_\nu}\int_{\oplus}\mathrm{d}^3\vec{r}\,'\frac{a(\vec{r}\,')\rho(\vec{r}\,')P(E_\nu,|\vec{r}-\vec{r}\,'|)}{4\pi|\vec{r}-\vec{r}\,'|^2} \tag{3}$$

where A is the decay rate per unit mass, $\mathrm{d}n(E_\nu)/\mathrm{d}E_\nu$ is the energy spectrum of neutrinos per decay, $\rho(\vec{r}\,')$ is the rock density, and $P(E_\nu,|\vec{r}-\vec{r}\,'|)$ is the neutrino survival probability after traveling from the source position $\vec{r}\,'$ to the detector position $\vec{r}$. The neutrino survival probability is given by a well-established formula,

$$P(E_\nu,L) \cong 1-\sin^2 2\theta_{12}\sin^2\left(\frac{1.27\Delta m^2_{12}[\mathrm{eV}^2]L[\mathrm{m}]}{E_\nu[\mathrm{MeV}]}\right) \tag{4}$$

where $L=|\vec{r}-\vec{r}\,'|$. In order to evaluate the geoneutrino rate detectable by KamLAND, we constructed a model of the Earth (Enomoto, 2005a, b). The model is based on the BSE composition given by McDonough (McDonough and Sun, 1995) and a crustal composition model given by Rudnick and Fountain (1995). Following common practice, we assume that the core does not contain U and Th. The mantle composition is assumed to be uniform and is obtained by subtracting the crustal composition from the BSE composition. With this Earth model, the geoneutrino flux at the KamLAND site (36° 25′36″ N, 137°18′43″ E, 358 m elevation from the sea level) is calculated to be 2.34×10^6 cm^{-2}sec^{-1} from ^{238}U decay, 0.07×10^6 cm^{-2}sec^{-1} from ^{235}U decay, 1.99×10^6 cm^{-2}sec^{-1} from ^{232}Th decay, and 1.48×10^6 cm^{-2}sec^{-1} from ^{40}K decay. As shown in Figure 2, about half of the total geoneutrino flux originates within 500 km radius, and about a quarter comes from the mantle. By modifying the Earth model, we found that re-distribution of the sources between the upper and lower mantle makes 3% variation to the total

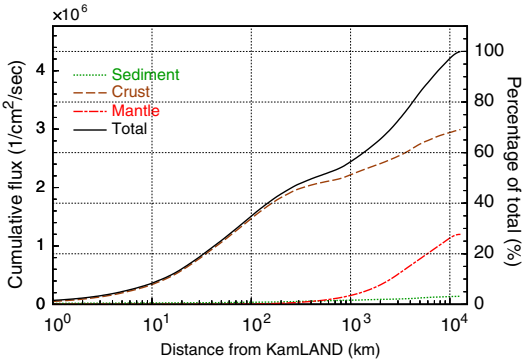

Figure 2. The expected ^{238}U and ^{232}Th geoneutrino flux within a given distance from KamLAND. Approximately 25 and 50% of the total flux originates within 50 km and 500 km of KamLAND, respectively. The mantle contributes 27% of the total flux.

flux, and alternation of the crustal models (i.e., adopting other crustal models (McLennan and Taylor, 1999; Wedepohl, 1995) with keeping the BSE composition by adjusting the mantle composition) makes 8% variation in the total flux (for details, see Enomoto, 2005a, b). The model parameters and the calculated flux contribution from each part of the Earth are summarized in Table II.

Due to large contribution from the near-field region, regional geological effect may considerably influence the total geoneutrino flux, while not significantly affecting the global geophysics. An estimation of the Japan Island Arc crustal composition shows depletion of U and Th in the Japan crust, which leads to reduction of U and Th geoneutrino flux at the KamLAND site by 6.4% and 8.4%, respectively. Based on a large scale geochemical study, the near-field surface geological non-homogeneity might affect the total flux at about 3–10%. Other regional geological effects, such as subducting plate and stagnant slab beneath Japan, Sea of Japan geology, Kamioka mine (where the KamLAND detector is located) geology, possible undiscovered uranium deposits, are estimated and found to affect the total flux at less than few percent (Enomoto, 2005a, b). In addition to the geological uncertainties, the uncertainty of the neutrino oscillation parameters makes 6% error in the flux estimation.

KamLAND detects electron antineutrinos via neutron inverse beta-decay,

$$\bar{\nu}_e + p \rightarrow \mathrm{e}^+ + n \tag{5}$$

which has a 1.8 MeV neutrino energy threshold, and a well-established cross-section (Vogel and Beacom, 1999). Only antineutrinos emitted from the ^{238}U and ^{232}Th decay series have energy higher than this threshold energy. The number of geoneutrino events from the reaction for the ^{238}U and ^{232}Th antineutrinos are calculated by

TABLE II

Reference Earth model and geoneutrino flux at Kamioka. U and Th concentrations, a_{element}, represent the geochemical model of the Earth, and the values $\Phi^{\text{Kamioka}}/L_{\bar{\nu}}^{\text{Reservoir}}$ are determined only from the geometrical shape of the reservoirs

Reservoir		a_{element} (ppm)		$\Phi^{\text{Kamioka}}/L_{\bar{\nu}}^{\text{Reservoir}} \times 10^{-19}(1\,\text{cm}^{-2})$	$\Phi^{\text{Kamioka}} \times 10^{5}(1\,\text{cm}^{-2}\text{s}^{-1})$	
		U	Th		^{238}U	^{232}Th
Sediment	Continental	2.8	10.7	3.16	0.61	0.51
	Oceanic	1.7	6.9	2.61	0.14	0.12
Continental Crust	Upper	2.8	10.7	8.34	11.5	9.57
	Middle	1.6	6.1	4.93	4.31	3.57
	Lower	0.2	1.2	4.97	0.53	0.69
Oceanic Crust		0.10	0.22	2.25	0.09	0.04
Mantle	Upper	0.012	0.048	2.31	2.20	1.91
	Lower	0.012	0.048	1.53	4.03	3.51
Core	Outer	0	0	1.24	0	0
	Inner	0	0	1.17	0	0
Bulk Silicate Earth (BSE)		0.02	0.08	3.89	23.4	19.9

$$N = N_{\text{proton}} \cdot \tau \cdot \varepsilon \cdot \int \mathrm{d}E_\nu \sigma(E_\nu) \frac{\mathrm{d}\Phi(E_\nu)}{\mathrm{d}E_\nu} \tag{6}$$

where N_{proton} is the number of target protons, τ is the detector exposure time, ε is the detection efficiency, and $\sigma(E_\nu)$ is the cross-section of the reaction. With 1-year exposure of 10^{32} target protons assuming 100% efficiency, one ^{238}U-neutrino event corresponds to a flux of 7.67×10^4 cm^{-2}s^{-1}, and one ^{232}Th-neutrino event corresponds to a flux of 2.48×10^5 cm^{-2}s^{-1}.

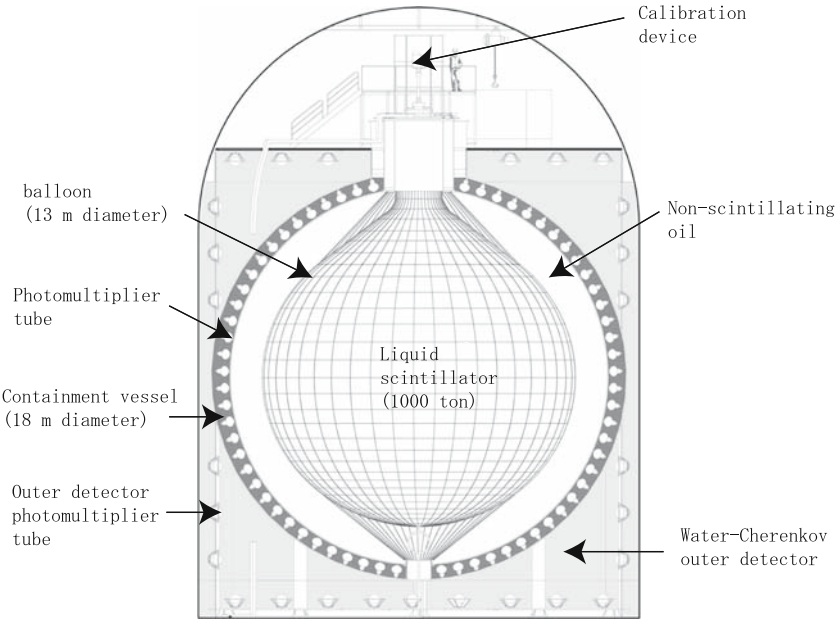

Figure 3. Schematic diagram of the KamLAND detector. The neutrino target/detector is 1000 ton of ultra-pure liquid scintillator (LS, 1,2,4-trimethylbenzene 20%, dodecane 80%, PPO 1.52 g/l) contained in a 13-m-diameter spherical plastic balloon (135-μm-thick transparent nylon/EVOH composite film). The balloon is supported and constrained by a network of Kevlar ropes. A buffer of dodecane and isoparaffin oils between the balloon and an 18-m-diameter spherical stainless-steel containment vessel shields the LS from external radiation. The specific gravity of the buffer oil is adjusted to be 0.04% lower than that of the LS. An array of 1879 photomultiplier tubes (PMT's) are mounted on the inner surface of the containment vessel. The array includes 1325 specially developed fast PMT's with 17-inch-diameter photocathodes and 554 older Kamiokande 20-inch PMT's. While the total photo-cathode coverage is 34%, only the 17-inch PMT's corresponding to 22% coverage are used for this geoneutrino analysis. A 3-mm-thick acrylic barrier at 16.6-m diameter helps prevent radon emanating from PMT grass from entering the LS. The containment vessel is surrounded by a 3200 ton water-Cherenkov detector with 225 20-inch PMT's. This outer detector absorbs gamma-rays and neutrons from the surrounding rock and provides a tag for cosmic-ray muons.

2. The KamLAND Detector

KamLAND is located in the Kamioka mine, 1000 m below the summit of Mt. Ikenoyama, Gifu prefecture, Japan (36°25′36″ N, 137°18′ 43″ E, 2700 m.w.e. underground) (http://www.awa.tohoku.ac.jp/KamLAND). The detector consists of 1000 ton of ultra-pure liquid scintillator (1,2,4-trimethylbenzene 20%, dodecane 80%, and PPO 1.52 g/l) surrounded by 1879 photo-multiplier tubes (PMT), 1325 of which are specially developed fast 17-inch PMT's and 554 of which are older Kamiokande 20-inch PMT's. Figure 3 illustrates the detector construction. The light output of the liquid scintillator is about 8000 photons/MeV, and the photo-coverage of the 1879 PMT's is 34%, providing ~500 p.e./MeV. For the geoneutrino analysis presented in this paper, only 17-inch PMT's are used, corresponding to 22% photo-coverage. The liquid scintillator was purified by the water extraction technique, resulting in very low radioactive impurity level ($(3.5 \pm 0.5) \times 10^{-18}$g/g for U, $(5.2 \pm 0.8) \times 10^{-17}$g/g for Th). The large light output and the low radioactive impurity level enable us to detect few MeV of antineutrinos. Together with the large volume, the KamLAND detector has attained the first sensitivity for geoneutrinos.

Electron antineutrinos are detected by the inverse beta-decay reaction (5). The reaction makes two correlated events. 'Prompt event', which is produced by the position, gives an estimate of the incident neutrino energy, $E_\nu \approx E_{e^+} + 0.8$MeV, where the E_{e^+} is the kinetic energy of the positron plus the electron-positron annihilation energy. With a mean time of ~200 μs, the neutron is captured by a proton, producing a deuteron and a 2.2 MeV gamma-ray ('delayed event'). The coincidences between the prompt and delayed events provide an effective way to reduce background.

Event positions are reconstructed based on PMT hit time distributions. Event energies (visible energy, or light yield) are determined from the amount of detected light after correcting for spatial dependences of the detector response. Particle energies are then calculated from the visible energy considering scintillator response (quenching) and Cherenkov light emission. The event position and energy determination are calibrated with gamma-ray sources deployed along the vertical center axis of the detector. Within the geoneutrino energy range (0.9 MeV $< E_{\text{visible}} < 2.6$ MeV, where E_{visible} roughly corresponds to E_{e^+}), positions and energies are determined within 5 cm and 2% accuracy, respectively, throughout the spherical volume of 5 m radius from the detector center. The scintillator mass in the 5 m radius spherical fiducial volume is estimated using reconstructed vertices of uniformly distributed cosmogenic events (^{8}B and ^{9}Li) and the measured total scintillator mass. The number of target protons in the fiducial volume is estimated at $(3.46 \pm 0.17) \times 10^{31}$.

2.1. Data analysis

The data presented here are based on a total detector live-time of 749.1 days after basic data quality cuts. The total exposure is $(7.09 \pm 0.35) \times 10^{31}$ target-proton years (Araki et al., 2005b). Neutrino event candidates are selected by searching for prompt events accompanied with a single 2.2 MeV delayed event. The time coincidence between the prompt and delayed events (ΔT) is required to satisfy $0.5\mu\,\mathrm{s} \leq \Delta T < 500\mu\,\mathrm{s}$, and the spatial coincidence between the prompt and delayed (Δr) is required to satisfy $\Delta r < 100$ cm. The delayed event energy (E_d) is required to satisfy $|E_\mathrm{d} - 2.2\mathrm{MeV}| < 0.4\mathrm{MeV}$, taking account of the detector energy resolution. The energy window for the prompt events of the geoneutrino candidates is set to $0.9\mathrm{MeV} \leq E_{e^+} < 2.6$ MeV, which corresponds to the neutrino energy of $1.7\mathrm{MeV} \leq E_\nu < 3.4$ MeV (the energy range reaches below the inverse beta-decay threshold owing to the detector energy resolution). The overall efficiency for detecting geoneutrino candidates within this energy window in the 5 m radius spherical fiducial volume is estimated to be 0.687 ± 0.007. To reject cosmogenic backgrounds, whole volume or partial volume vetoes are applied following the passage of every cosmic muon. The deadtime due to the vetoes, 10.5% of the total run time, is subtracted from the live-time.

Background for geoneutrino candidates is dominated by antineutrinos from nuclear reactors in the vicinity of the KamLAND detector, and by alpha-particle induced neutrons due to radioactive contamination within the detector. As shown in Figure 4a, reactor neutrinos reach substantially higher energies than geoneutrions, and the properties of the reactor antineutrinos have been studied in detail using this energy region (Eguchi, 2003; Araki et al., 2005). Using the neutrino oscillation parameters determined with antineutrinos in the $E_\nu > 3.3$ MeV region, together with the global analysis of the solar neutrinos (assuming CPT invariance), the reactor antineutrino background in the geoneutrino analysis window is estimated to be 80.4 ± 7.2. The error is dominated by the neutrino oscillation parameter uncertainties, and the initial reactor neutrino flux was calculated within a 3% error.

The alpha-particle-induced neutron background is due to the $^{13}\mathrm{C}(\alpha, n)^{16}\mathrm{O}$ reaction, where the alpha particle is produced in the ^{210}Po decay. The initial energy of the alpha particle emitted by the ^{210}Po decay is 5.3 MeV, and the $^{13}\mathrm{C}(\alpha, n)^{16}\mathrm{O}$ reaction produces neutrons with kinetic energy up to 7.3 MeV. The neutrons scatter protons as they thermalize, and the scattered protons yield scintillation light with a total visible energy of few MeV. Here the visible energy is much smaller than the initial neutron kinetic energy owning to scintillation light quenching for high ionization density. The thermal neutrons are captured by protons and produce a 2.2 MeV delayed gamma signal, in exactly the same way as neutrons produced by the inverse beta decay reaction.

^{210}Po's is produced by decay of ^{210}Pb, which has a half-life of 22 years. ^{210}Pb's is populated throughout the whole scintillator volume from the decay of ^{222}Rn, which might have been injected into the liquid scintillator during the detector construction process. Non-equilibrium of the ^{210}Po decay rate implies that ^{210}Pb could be populated during a short period of scintillator filling into the detector, and an estimation of the initial amount of ^{222}Rn based on this assumption resulted in about 100 Bq/m^3, which is more than the maximum amount under contact of the liquid scintillator with atmospheric air (Note that Rn concentration in the mine air is much higher than atmospheric air).

On the basis of the ^{13}C(α, n)^{16}O reaction cross-section, the alpha-particle energy loss in the scintillator, and the number of ^{210}Po decays, the total number of neutrons produced is calculated to be 93 ± 22, where the error is dominated by 20% uncertainty in the ^{13}C(α, n)^{16}O reaction cross-section and 14% uncertainty on an estimation of the ^{210}Po decay rate. The neutron energy distribution is calculated using a ^{13}C(α, n)^{16}O neutron angular distribution data. The visible energy spectrum is then calculated with neutron–proton scattering simulation and an estimated quenching factor for protons, assigning reasonably large error (10% in energy determination) for uncertainties in the quenching factor estimation. Including the efficiency for passing the neutrino selection cuts, the number of ^{13}C(α, n)^{16}O events is estimated to be 42 ± 11.

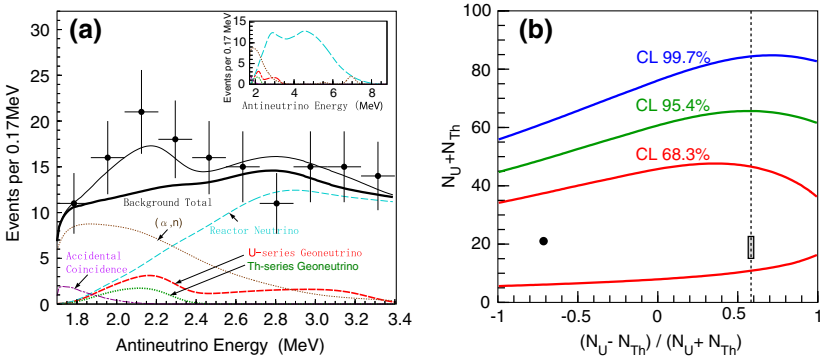

Figure 4. Neutrino energy spectra in KamLAND (left) and spectrum shape analysis result (right). Panel (a) shows the experimental points together with the total expectation (thin solid line), the total expected spectrum excluding the geoneutrino signal (thick solid line), and the expected spectra of the background signals. The geoneutrino spectra are calculated from our reference Earth model, which is based on the BSE model. In panel (b), the 68.3, 95.4, and 99.7% confidence level contours for detected ^{238}U and ^{232}Th geoneutrinos are shown. The small shaded area represents the prediction from the reference Earth model. The vertical dashed line represents the value of $(N_U - N_{Th})/(N_U + N_{Th})$ assuming the mass ratio of Th/U = 3.9. The dot represents our best fit point, favoring 3 ^{238}U geoneutrinos and 18 ^{232}Th geoneutrinos.

The contribution from accidental coincidences is 2.38 is eliminated as small as 2.38 ± 0.01 events, by adopting tighter neutrino-selection criteria with a smaller radius fiducial volume than used for the reactor neutrino analysis (Araki et al., 2005a). There is a small contribution to the background from decays of cosmic-muon-induced unstable nuclei such as ^{9}Li (which has a neutron in the final state), and neutrinos from spent reactor fuel. There is a negligible contribution from fast neutrons generated by cosmic ray interactions and spontaneous fission of ^{238}U. Other background sources considered and found to be negligible include neutron emitters and correlated decays in the radioactive impurities, (γ, n) reactions, solar neutrino induced break-up of ^{2}H, and cosmic neutrino interaction with scintillator-composing nuclei. The total number of background events is estimated to be 127 ± 13.

The total number of observed antineutrino candidates within the energy range of $1.7\text{MeV} \leq E_{\nu} < 3.3\text{MeV}$ is 152. The error on the geoneutrino detection efficiency is estimated at 5.0%, which is dominated by the fiducial volume determination uncertainty (4.9%). Including the detection systematic errors, part of which are correlated with the background estimation errors, a 'rate-only' analysis gives 25^{+19}_{-18} geoneutrino candidate events. Dividing by the detection efficiency, live-time, and number of target protons, the total geoneutrino rate obtained is 51^{+39}_{-36} per 10^{32}-protons per year.

Figure 4a shows the observed neutrino candidate event energy spectrum, the estimated background spectra, and the expected geoneutrino spectra calculated based on our Earth model. The confidence intervals for the number of observed geoneutrinos from an un-binned maximum likelihood analysis is shown in Figure 4b. As shown in the figure, KamLAND has sensitivity in determination of the total geoneutrino flux (vertical axis in the figure), while KamLAND is less sensitive in discrimination between the U-series and Th-series geoneutrinos (horizontal axis in the figure). On the other hand, the Th/U mass ratios in the chondritic meteorites, the solar photosphere, and surface rock samples show stable value at around 3.9, and model estimations of the Th/U mass ratios in the bulk Earth, the crusts and the mantle, are relatively more reliable than the absolute concentrations of U and Th. Assuming a Th/U mass ratio of 3.9, the 90% confidence interval for the total number of geoneutrino candidates is estimated to be 4.5–54.2, with a central value of 28.0. The 99% C.L. upper limit is given at 70.7 events, which corresponds to 145 geoneutrinos per 10^{32}-protons per year and a flux of 1.62×10^{7} cm^{-2}s^{-1}.

3. Discussion

One of the primary interests of geoneutrino observation is to determine the Earth's global heat budget (i.e., direct test of the BSE model). As mentioned previously, the dependence of the flux on the crustal and mantle modeling is about the same order of magnitude as the current uncertainty of the BSE composition. Figure 5 shows the relation between the U and Th amount in each reservoir of the Earth and the geoneutrino flux from each reservoir, calculated with our reference Earth model. In the figure, alternation of reservoir's composition moves the corresponding point along the diagonal line (the slope of which is determined by the geometrical shape of the reservoir and the detector position), and the total geoneutrino flux from all of the reservoirs is obtained as a simple vector sum of each reservoir point. Assuming that we scale concentrations of U and Th in all reservoirs equally, the total geoneutrino flux observed with KamLAND $F_{\mathrm{U+Th}}$ is related to the total ^{238}U and ^{232}Th mass in the Earth $M_{\mathrm{U+Th}}$ and the heat generation $H_{\mathrm{U+Th}}$ as

$$H_{\mathrm{U+Th}}[\mathrm{TW}] = \frac{M_{\mathrm{U+Th}}[\mathrm{kg}]}{2.49 \times 10^{16}} = \frac{F_{\mathrm{U+Th}}[\mathrm{cm^{-2}s^{-1}}]}{2.70 \times 10^{5}}. \tag{7}$$

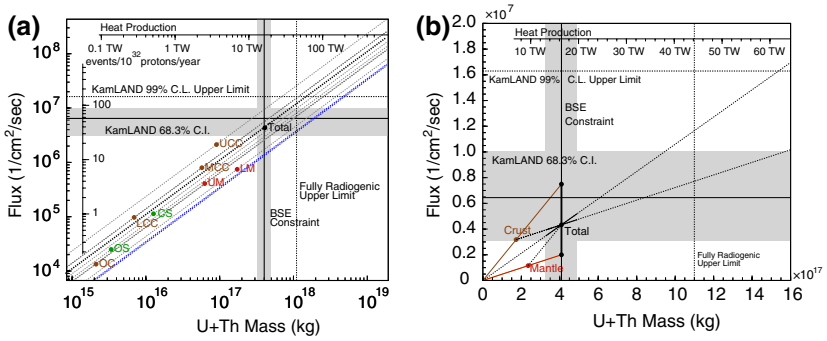

Figure 5. Comparison with Earth model predictions. Both figures show the same values but in a different axis scaling and different reservoir classification. The horizontal line is the KamLAND best-fit flux and the horizontal shaded band shows the interval of 68.3% C.L. The horizontal dotted line is the 99% C.L. upper limit. The points represent the expected neutrino flux at the KamLAND site in the reference Earth model; Upper Continental Crust (UCC), Middle Continental Crust (MCC), Lower Continental Crust (LCC), Oceanic Crust (OC), Continental Sediment (CS), Oceanic Sediment (OS), Upper Mantle (UM), and Lower Mantle (LM). This assumes a Th/U ratio of 3.9. The auxiliary axis on the top shows heat generation from U and Th for a given U + Th mass.

Therefore the observed geoneutrino flux corresponds to 23^{+13}_{-12} TW of the total radiogenic heat by ^{238}U and ^{232}Th decays. If we fix the crustal composition and parameterize the mantle composition as another example, the relation becomes

$$H_{\mathrm{U+Th}}[\mathrm{TW}] = \frac{M_{\mathrm{U+Th}}[\mathrm{kg}]}{2.49 \times 10^{16}} = 6.58 + \frac{(F_{\mathrm{U+Th}}[\mathrm{cm}^{-2}\mathrm{s}^{-1}] - 31.7 \times 10^{5})}{1.22 \times 10^{5}}. \quad (8)$$

In this case the observed geoneutrino flux corresponds to 33^{+30}_{-28} TW of the total radiogenic heat. Relations under other constraints can be directly obtained from the points and lines in Figure 5 and/or the numbers listed in Table II in the same way.

The 99% C.L. flux upper limit is 3.8 times higher than the predicted flux based on the reference Earth model, which gives 16 TW of total radiogenic heat from U and Th. Since the 99% C.L. flux upper limit is far above the predictions from Earth models due to limited statistics, we do not expect that any realistic Earth models can be used to translate this large flux to heat production. However, if we simply scale the heat production with relation (7) just to show the possible effect that geoneutrino data would have on geophysical thermal constraints, then the 99% C.L. flux upper limit is translated to a heat production of 60 TW.

The current KamLAND observation (confidence interval and 99% upper limit) is shown in Figure 5. The observation is in agreement with our Earth model prediction based on the BSE composition, although the measurement errors are relatively large. Even if the current KamLAND observation is not as precise as predictions or limits by Earth models, one can see that geoneutrino observation is approaching the point where we can gain fruitful geophysical information with geoneutrinos.

3.1. Future prospects

The current KamLAND observation suffers from large background originating from the reactor antineutrinos and (α, n) reactions. In particular, the contribution from the (α, n) reaction background is poorly estimated due to large uncertainties of the ^{210}Po decay rate, (α, n) cross-section $\sigma(E)$, (α, n) partial cross-section $\mathrm{d}\sigma(E, \theta)/\mathrm{d}\Omega$ where θ is the neutron scattering angle, and the neutron (or proton) quenching factor.

In order to reduce the uncertainty on ^{210}Po decay rate, we have improved the event reconstruction tool, resulting in a small bias in the low energy and large R (i.e., near the boundary of the fiducial volume) region. A new measurement of the (α, n) total cross-section is now available (Harissopulos,

2005), which reduces the error on the total cross-section from 20% to 4%. In order to understand the liquid scintillator response to protons, we have performed a measurement with a mono-energetic neutron beam. A new calibration source, which consists of an α source and ^{13}C, is being prepared. In summary, we will have a better understanding of the (α, n) background process and will be able to reduce one of the largest uncertainties of geo-neutrino observation.

For the next phase of the KamLAND experiment, which primarily aims for real-time observation of ^{7}Be solar neutrinos, a new purification system is being constructed. This system is beneficial for geoneutrions measurement, since it reduces background due to accidental coincidences and (α, n) to a negligible level. Reduction of accidental coincidences may allow extending the fiducial volume and improving the detection efficiencies by relaxing the delayed coincidence event selection criteria.

We estimated prospects of future KamLAND geoneutrino observation after purification by applying the same analysis method as used for the current geoneutrino analysis (Araki et al., 2005b) to software-generated neutrino event candidates. An extended fiducial volume of 5.5 m radius together with an improved detection efficiency of 99% are used, which are the values currently implemented in the KamLAND reactor neutrino analysis (Araki et al., 2005a). Figure 6 shows the expected analysis results after 750 days exposure of the detector, which is the same period as used in the current KamLAND geoneutrino result. KamLAND can determine the geoneutrino flux within 35% accuracy, which is a great improvement from

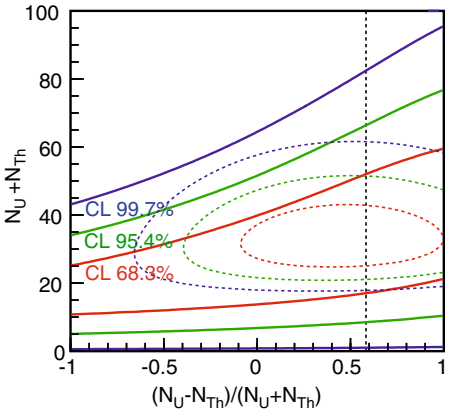

Figure 6. Prospects of future KamLAND geoneutrino observation after purification. The same analysis method as used for the current analysis is applied, except for reduced radioactive background estimation and consequent selection criteria relaxation. The solid lines show the 68.3, 95.4, and 99.7% confidence level contours. The dotted lines show the same analysis of prospects, except for absence of reactor neutrino background.

the current 54% accuracy. The significance of positive geoneutrino signal may reach 99.96%. If we combine it with the current data, the accuracy becomes 28%, which is comparable with the model prediction uncertainty. The 99% flux upper limit may be given at around 30 TW heat-generation-equivalent, which is below the surface heat-flow measurement results (44.2 ± 1.0 TW (Pollack, 1993)). Separation of ^{238}U and ^{232}Th neutrinos seems to be still difficult due to large backgrounds from the surrounding nuclear power reactors, as shown in the figure by the contrast between the contours with and without the reactor background.

4. Conclusion

The measurement of antineutrinos with an exposure of $(7.09 \pm 0.35) \times 10^{31}$ target-proton years of KamLAND is the first experimental study of geoneutrinos. The present measurement is consistent with our model predictions based on the bulk silicate Earth composition, and sets an 99% C.L. upper limit of the geoneutrino flux from ^{238}U and ^{232}Th decays within the Earth at 1.62×10^7 cm^{-2}s^{-1}, which scales to 60 TW of radiogenic heat production equivalent. Further exposure with improved accumulation of statistics with improved analysis method, reduced systematic error, and removal of radioactive background sources by the newly installed purification system will provide more precise determination of the geoneutrino flux, which might be comparable with uncertainties in the Earth models. The current result of KamLAND demonstrates that geoneutrinos are practical new tool to study the Earth interior, and paves the way to future, more accurate measurements.

References

Aleksankin, V. G. et al. 1989, in P. M. Rubzov (ed.), *Beta and Antineutrino Radiation of Radioactive Nuclei*, Energoatomizdat, Moscow, 719 pp.

Araki, T. et al. [KamLAND Collaboration]: 2005a, *Phys. Rev. Lett.* **94**, 081801.

Araki, T. et al. [KamLAND Collaboration]: 2005b, *Nature* **436**, 499–503.

Avilez, C., Marx, G. and Fuentes, B.: 1981, *Phys. Rev. D* **23**, 1116–1117.

Eder, G.: 1966, *Nucl. Phys.* **78**, 657–662.

Eguchi, K. et al. [KamLAND Collaboration]: 2003, *Phys. Rev. Lett.* **90**, 021802.

Enomoto, S.: 2005a, Neutrino Geophysics and Observation of Geo-Neutrinos at KamLAND, Thesis, Tohoku Univ.; available at http://www.awa.tohoku.ac.jp/KamLAND/publications/Sanshiro_thesis.pdf.

Enomoto, S. et al.: 2005b, Neutrino Geophysics with KamLAND and future prospects, submitted, arXiv:hep-ph/0508049.

Firestone, R. B. and Shirley, V. S.: 1996. *Table of Isotopes* (8th ed.). John Wiley, New York.

Harissopulos, S. et al.: 2005, *Phys. Rev. C* **72**, 062801.

http://www.awa.tohoku.ac.jp/KamLAND/.

Kobayashi, M. and Fukao, Y.: 1991, *Geophys. Res. Lett.* **18**, 633–636.
Krauss, L. M., Glashow, S. L. and Schramm, D. N.: 1984, *Nature* **310**, 191–198.
Mantovani, F. et al.: 2004, *Phys. Rev. D* **69**, 013001.
Marx, G.: 1969, *Czech. J. Phys. B* **19**, 1471–1479.
McDonough, W. F. and Sun, S.-s.: 1995, *Chem. Geol.* **120**, 223–253.
McLennan S. M. and Taylor S. R.: 1999, in Marshall C. P. and Fairbridge R. W. (eds.), *Encyclopedia of geochemistry*, Kluwer Academic Publishers, Dordrecht, The Netherlands, pp. 145–150.
Pollack, H. N. et al.: 1993, *Rev. Geophys.* **31**, 267–280.
Raghavan, R. S. et al.: 1998, *Phys. Rev. Lett.* **80**, 635–638.
Rothschild, C. G., Chen, M. C. and Calaprice, F. P.: 1998, *Geophys. Res. Lett.* **25**, 1083–1086.
Rudnick, R. L. and Fountain, D. M.: 1995, *Rev. Geophys.* **33**, 267–309.
Vogel, P. and Beacom, J. F.: 1999, *Phys. Rev. D*, **60**, 053003.
Wedepohl, K. H.: 1995, *Geochem. Cosmochem. Acta* **59**, 1217–1232.